Radiance Values Inside Lunar Caves and Lava Tubes

G. Rodeghiero*[1] [a,b], Claudio Pernechele[c], Matteo Munari[d], Riccardo Pozzobon[c,e], Maurizio Pajola[c], Ivan Di Antonio[b], Alice Lucchetti[c], Matteo Massironi[e], Emanuele Simioni[c], Dorit Borrmann[f], Francesco Maurelli[g], Andreas Nüchter[f] and Angelo Pio Rossi[h]

[a]INAF Astrophysics and Space Science Observatory of Bologna, Plesso del Battiferro, Via Gobetti 93/3 Bologna, Italy; [b]INAF Astronomical Observatory of Abruzzo, Via Mentore Maggini snc, Loc. Collurania, 64100 Teramo, Italy; [c]INAF OAPD, Astronomical Observatory of Padova, Vicolo Osservatorio 5 - 35122 Padova, Italy; [d]INAF Astrophysical Observatory of Catania, Via Santa Sofia 78, 95123 Catania, Italy; [e]UNIPD, Department of Geosciences, Via G. Gradenigo, 635131 Padova, Italy; [f]Julius Maximilian University of Würzburg - Informatics VII: Robotics and Telematics, Am Hubland, 97074 Würzburg, Germany; [g]Department of Computer Science and Electrical Engineering, Jacobs University Bremen, Campus Ring 1, 28759 Bremen, Germany; [h]Department of Physics and Earth Sciences, Jacobs University Bremen, Campus Ring 1, 28759 Bremen, Germany

ABSTRACT

There is currently a growing interest for the in-situ robotic and human exploration of the Moon's surface and subsurface. In particular, several mission concepts foresee the exploration of lunar caves and underground structures like e.g. the lava tubes, (i.e. conduit formed by flowing lava from a volcanic vent that moves beneath the hardened surface of a lava flow) and other depressed morphologies such as permanently shadowed craters which could present in situ resources such as water ice. Given the limited onboard resources of these missions and extreme illumination conditions ranging from sunlight to complete darkness, the cameras might be capable of operating without the support of any artificial illumination system. This paper studies the radiance properties of a set of different lunar cave pits as illuminated uniquely by the sunlight for different Sun elevations above the Moon horizon and permanently shadowed craters such as Shackleton's interior. This is as an endmember for complete darkness of extreme importance because it could be a cold trap for volatiles and a potential future human exploration target. The simulations are carried out using the OpticStudio ray tracing software and a Lambertian scattering model of the cave pit walls. The radiance maps within the caves can be used by the scientific community to estimate the typical Signal to Noise Ratio (SNR) of the required observations with optical cameras deployed on the lunar surface. This is accomplished both for directly illuminated, penumbra and umbra regions of the cave pit. We believe that the proposed investigations are of wide interest for the future missions to the Moon and its robotic and manned exploration.

Keywords: Cave, Moon, radiance, scattering.

1. INTRODUCTION

The revived interest for the robotic and human exploration of the Moon is leading to innovative mission scenarios and new Moon-based infrastructures for human life support systems, in-situ energy identification as well as raw materials extraction and research facilities [1]. The lunar gateway [2] will be the first step bringing humans back to the Moon surface and paving the ground for the permanent exploration of our satellite. In this context, many scientific missions will deploy optical instruments on the Moon surface. Among them some will be craned down or rolled off a lunar cave for in situ 3D mapping and rock sampling [3]. The lunar environment is harsh and poses several constraints on the

[1] *gabriele.rodeghiero@inaf.it; phone +39 051 6357315

scientific mission design. An example for the instrumentation to explore the lunar caves is the limited amount of onboard energy available to the payload. The optical cameras craned down into the lunar caves shall be capable of operating without any artificial light source to illuminate the scene, which has conditions that can range from full illumination to complete darkness in a few meters. To reach a good Signal to Noise Ratio (SNR) within an exposure frame is therefore pivotal to understand the level of natural illumination within the cave. Indeed, the cave walls can be either directly illuminated by the Sun or indirectly illuminated as a result of the scattering of the sunlight by a fraction of the pit wall towards another. A similar condition is most likely present on permanently shadowed craters. The level of natural illumination within a lunar cave can be described mathematically by the radiance which is a radiometric parameter that represents the radiant flux emitted or reflected by a surface, over a unit solid angle and a unit projected area ($W\ m^{-2}\ sr^{-1}$). The optical ray tracing simulations with a software like OpticStudio can reproduce typical caves' environments by modelling the cave optical surface properties in terms of their reflectance and scattering as a function of the wavelength. In this paper we report the radiance estimates for a set of nine different lunar caves. For each cave we quantify the expected radiance both for the side directly illuminated by the Sun and for the one in the shade. We then refer all these observations to an extreme case of a well-known permanently shaded depression such as the interior of Schackleton crater at the lunar South Pole as an endmember, although not being a lunar cave. This study can be used as a starting point for the evaluation of the instruments performance like the expected SNR and the suitable exposure time for the scientific frames in extreme lighting conditions.

2. THE LUNAR CAVE SCIENCE AND PERMANENTLY SHADOWED CRATERS

The discovery in 2009 of the Marius Hills 65 m-size skylight with the JAXA/SELENE-Kaguya Terrain Camera [4] opened new questions on the existence [5] formation processes [[6][7][8]], size and stability [[10][8][9]] of underground voids related to drained lava tubes. Before such direct proof, the existence and entity of such voids has been inferred to be up to hundreds of meters in height. This has been derived through i) radar sounder measurements at several locations (including Marius Hills [5]), ii) gravity mass deficits with GRAIL [11], as well as iii) comparative planetology with morphometric analysis of Earth analogues [8]. In particular, their stability has been addressed by structural stability models [[10][9]] suggesting that, theoretically, under lunar gravity conditions voids up to 1 km across can be stable under roofs with a maximum thickness of only a few meters. After Marius Hills and several other skylights discovery, such roof geometry has been imaged at different phase and incidence angles by NASA/Lunar Reconnaissance Orbiter Narrow Angle Camera. This wide imagery dataset showed that the lava-tube roofs are often overhanging and formed by several meter-thick layers of lava flows [12]. Therefore the accessibility of these caves could potentially provide, as in Earth analogues, stable temperatures with little to no variation across day and night cycles, micrometeorites impacts and shelter from radiation. The only known access to these voids are vertical shafts with overhanging roofs [19], whose thickness is variable. Nevertheless, a quantitative estimate of the environmental conditions, such as the illumination of these voids as well as their stability remains largely theoretical or inferred from comparative planetology (e.g. [13]).
In addition to all the above questions related to environmental and, eventually, habitability conditions, the in situ analysis of such pits could provide the possibility to derive an extremely important scientific return, during both the first close approach and the descent phase down the vertical shaft (e.g. [15]). Indeed, along the walls, the analysis at close-range of the stratigraphy of the stacked lava flows (which is present and well-visible as in [12]) will provide more insights both in terms of morphological characteristics of the lava layers, presence of paleoregolith, fracturing and compositional diversity. The reach of the bottom of the collapse pit and the possibility to assess environmental and morphological conditions of the underground tunnel is also of equal importance. Moreover, investigating the presence of volatiles and cold traps bearing water ice is pivotal for In-Situ Resource Utilization (ISRU) and further exploration. Hence, the accessibility and trafficability of such underground voids in the Moon globally harsh environment forces to carefully analyze the radiation environment, which is tightly connected and dependent on the illumination conditions inside such collapse pits. This impacts not only the thermal environment and the performance of the robotic systems but also it constrains how the payload needs to be designed and calibrated to perform effective and meaningful observations. Permanently shadowed craters are another extremely important case study where the techniques hereby exposed can be successfully applied and of extreme utility. Indeed these craters, which are present -for example- around the lunar South pole never receive direct sunlight and their only illuminated part is their inner rim until a certain depth threshold. Shackleton Crater [16] a ~20 km crater roughly coinciding with the lunar south pole, is a beautiful example of such type of craters. These are of extreme importance as they can represent "cold traps" for volatiles and water ice that could be exploited in future exploration. Moreover, they offer an effective endmember for studying such types of illumination

conditions and calibrate exposure and SNR time in order to obtain a meaningful instrumental performance for scientific investigation [17].

3. RAY TRACING SIMULATIONS

The approach followed to retrieve the radiance within the Moon cave pits is based on three different software tools. Once the collection of the lunar caves (see Table 1) has been recognized, the typical Sun elevation during a lunar cycle is calculated using the Systems Tool Kit (STK). The visibility between the Sun and a topocentric observer placed on the Moon surface in correspondence of the cave latitude and longitude is calculated by STK and the Sun elevation is stored with a time sampling of 5 minutes. An example of such a dataset for the Lacus Mortis cave is shown in Figure 1.

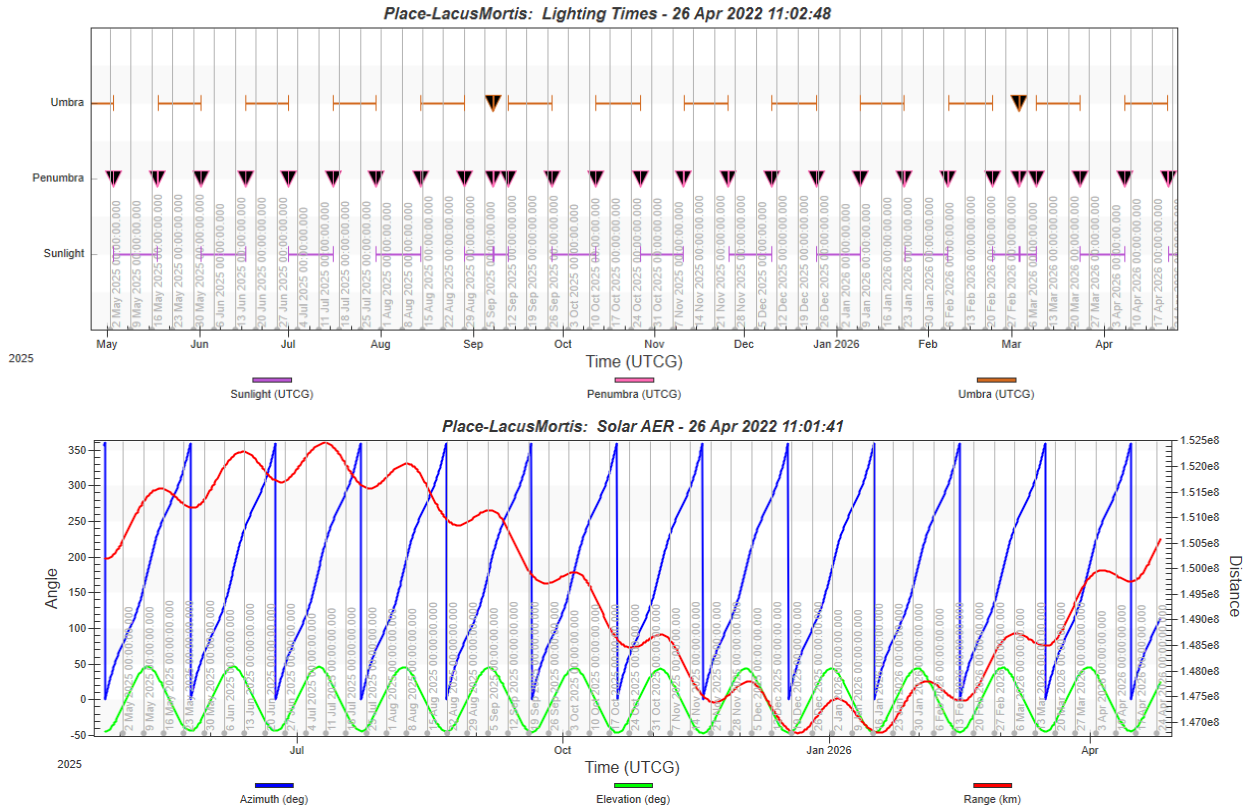

Figure 1 Example of dataset retrieved with STK: the software calculates the intervals of visibility between the Sun and the lunar observer at the cave (top) and the Sun coordinates in the lunar surface topocentric reference frame.

The Sun elevation data are used to model the light source orientation with respect to the cave pit in the OpticStudio ray tracing simulations. Each cave pit is modelled in a non-sequential OpticStudio design containing: the cave itself, an array of detectors (360 units) a light source (the Sun) and the cave outer funnel. The geometry of the different cave pits is reported in Table 1, they are represented either as cylinders or as elliptical cylinders. The position on the Moon surface of the caves is shown in the projection map of Figure 2. The base of the cave is represented as a slightly concave surface with a large radius of curvature (100m-200m). The cave pit, the base and the outer funnel have a Lambertian scattering profile with an albedo of 0.15 [18] and a gray reflectance profile (no wavelength dependance). The light source representing the Sun has flux of 1400 W/m^2 at 550 nm and its rays are traced for each elevation point equal or greater than 1 degree. The array of detectors populates the whole cave pit circumference and it extends vertically for the whole pit's depth. The detector array is placed 0.5 m inward with respect to the cave pit. For each Sun elevation position a complete ray tracing is run and the array detector data are collected and stored. The detectors settings are set in order to get only the back-scattered light from the pit walls and not the direct (unscattered) Sun light. Given the large amount of

Sun-to-cave configurations and the multiplicity of the caves, the simulations are automated using the Matlab ZOS-API functions that enable to drive OpticStudio from a Matlab environment where the different configurations can be accessed in a for loop. The orientation of the cave major and minor axes with respect to the lunar north has not been taken into account to limit the degrees of freedom of the simulations.

Table 1 Selection of lunar caves and the permanently-shaded Shackleton crater with their location and geometric parameters investigated in the current study. Adapted from [19]. In this study we have assumed the average depth value for the pits and funnel when a range of values is given.

Caves location	**Coordinates**	**Pit**	**Outer funnel**
	Latitude, Longitude	**Diameter(m) - Depth(m)**	**Diameter(m)-Depth(m)**
Lacus Mortis	44.962, 25.61	140x110 - 80	280x210 - 35
Central Mare Fecunditatis	-0.917, 48.66	130x110 - 30	190x160 - 15
Mare Tranquillitatis	8.335, 33.222	100x88 - 105	170x150 - 5-9
Mare Ingenii	-35.948, 116.053	100x68 - 45-65	160x130 - 15-20
Southwest Mare Fecunditatis	-6.752, 42.759	16x14 - 35	60x55 - 40
Marius Hills	14.091, 303.23	58x49 - 40	70x80 - 4-10
Hayn	64.6, 89.9	20x16 - 6	none
Schlüter Crater	-5.839, 276.95	40x40 - 25	55x55 - 15
Permanently shadowed craters	**Coordinates**	**Permanently shadowed crater portion**	**Outer illuminated rim**
Shackleton Crater	-89.9 - 0.0	15000x15000 - 3000	21000x21000 - 1000

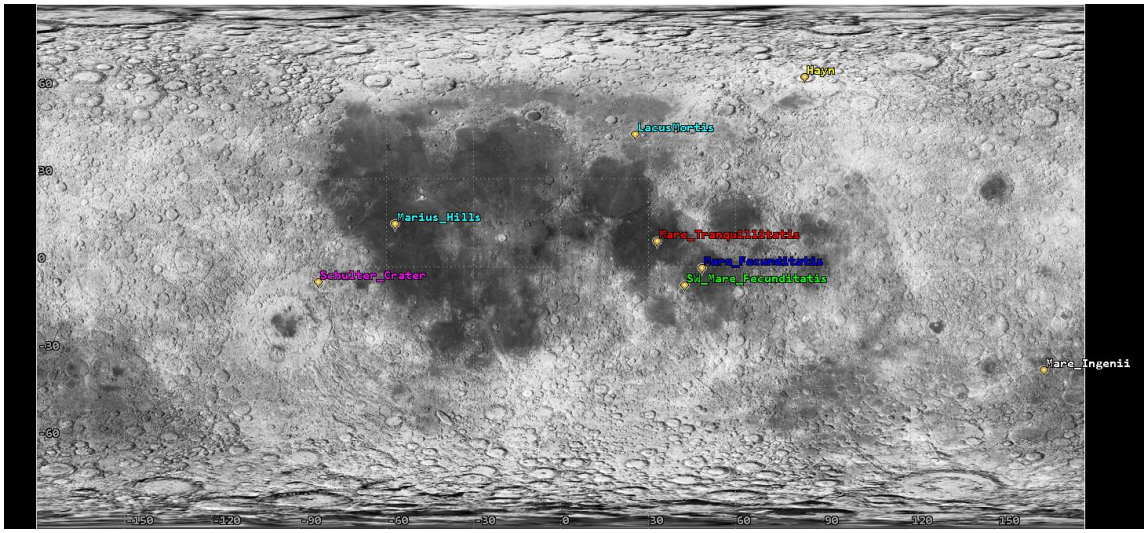

Figure 2 Position on the Moon surface of the cave pits considered in the study. The Shackleton Crater at the South Pole is not shown on the map.

The cave funnels and impact crater rims can have different shape profiles [19] that for convenience we have split into two main categories: an inner sloping funnel and a torus-like funnel as shown in Figure 3.

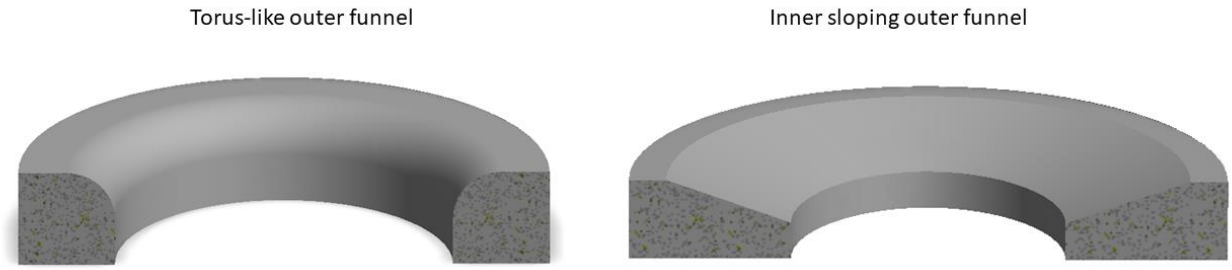

Figure 3 Two types of outer funnels geometries are simulated for the lunar pits, an inner sloping (right) and a torus-like rim (left).

4. RADIANCE WITHIN THE LUNAR CAVES

In this section we report the core of our findings retrieved using the simulation architecture that we introduced in the previous paragraph. As already mentioned, the surfaces of the cave walls, base and outer funnel have been described by a Lambertian scattering profile with a 1-to-1 probability ratio between parent and child ray, i.e. one incoming parent ray being scattered creates a scattered child ray towards a random direction with a unitary probability. The Lambertian model has no privileged direction of scattering and it is not influenced by the angle of incidence of the incoming ray. This behaviour is per se ideal since every material shows a residual preferred scattering direction towards an angle specular to the incoming ray angle of incidence. However for a rough material as the lunar regolith this scattering model assumption seems to be a good approximation of the real scenario. The threshold of ray traceability into the system is set to 10^{-6}: when the intensity of the scattered/reflected child ray reaches a relative ratio of 10^{-6} with respect to the initial, parent ray its propagation within the system is terminated. Considering the albedo of the cave surfaces at 0.15, the child ray is terminated after ~7 consecutive reflection/scattering events with the cave walls. The output of the automated Matlab ZOS-API procedure is a dataset of radiance maps within each cave as a function of the Sun elevation. An example of such maps is given in Figure 4. The unfolded map can be subdivided into two regions: the sunny side which is directly illuminated by the Sun, and the shade side which is illuminated only in virtue of the scattered sunlight by the sunny side of the cave.

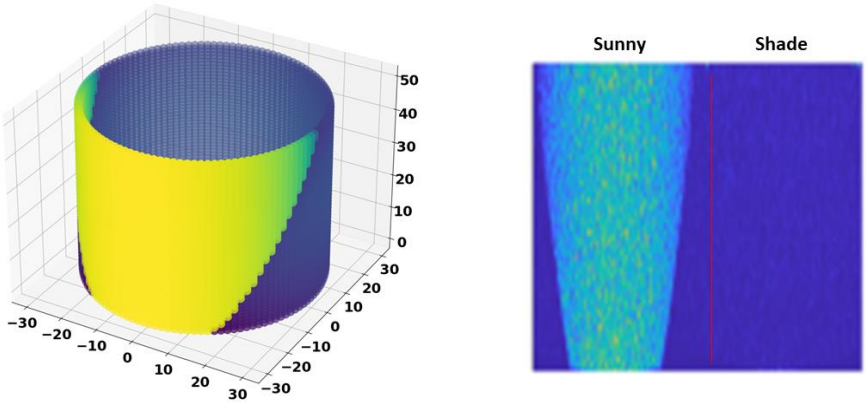

Figure 4 The detector array that covers the whole circumference of the cave pit is unfolded to create a projected radiance map of the cave pit where the sunny and shade regions are disentangled and suitable for a precise measurement and statistics of the radiance values in the two opposite regions.

The radiance of the cave pit walls during a two weeks period of direct sunlight illumination (Sun elevation > 1 deg) of the caves is reported in Figure 5 and Figure 6 for the sunny and shade side respectively. The figure of merit assumed for the analysis is the average value of the radiance in the two opposite sides of the cave pit.

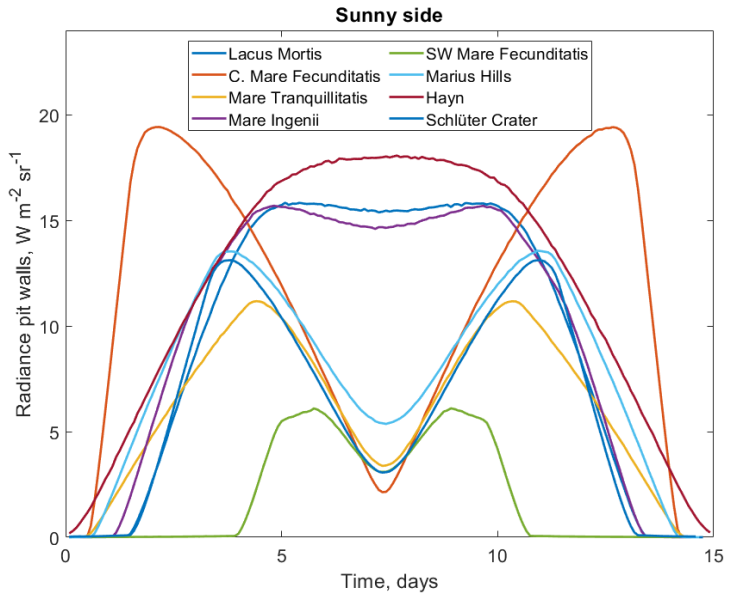

Figure 5 Average radiance from the sunny side of the cave pit during the two weeks of direct sunlight illumination. The shape of the radiance profile is strongly influenced by the Sun elevation.

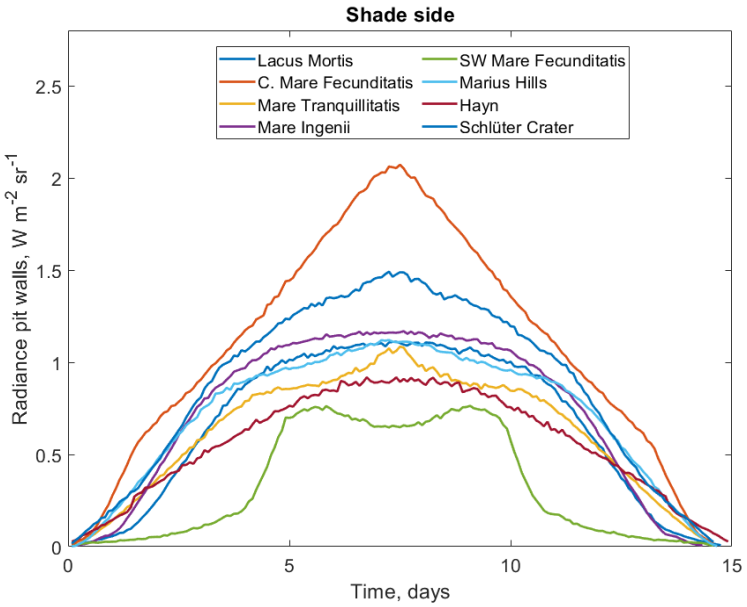

Figure 6 Average radiance from the shade side of the cave pit. The radiance of the shade side is entirely due to the sunlight scattered or reflected off the sunny side of the pit. The variation of the radiance profile among the different caves is less pronounced with respect to the sunny side (Figure 5).

The shape of the profile of the radiance of the sunny side is strongly influenced by the Sun elevation (Figure 7). The caves undergoing a high culmination of the Sun like the C. Mare Tranquillitatis, Mare Tranquillitatis, Schlüter Crater, SW Mare Fecunditatis and Marius Hills, show a double-peak profile of the radiance with time. Caves like the Mare Ingenii, Hayn and Lacus Mortis experience a lower elevation of the Sun at its culmination point and they present a smoother flat top-hat profile of the radiance from their sunny side. The Sun elevation therefore carves the profile of the

radiance from the sunny side of the pit. The behaviour of the radiance profile is confirmed also by the use of the median instead of the mean. The difference is well visible by comparing the Schlüter and Hayn Craters reported in Figure 8.

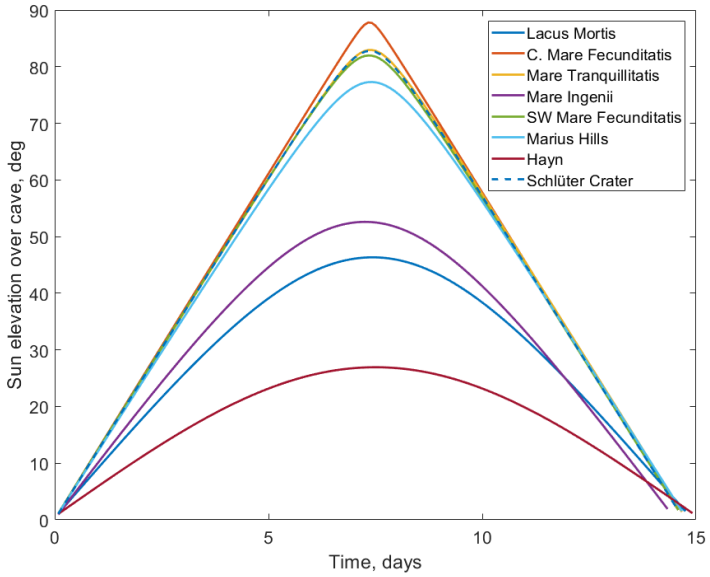

Figure 7 Sun elevation path as seen from a topocentric observer at the different cave locations. The caves at Lacus Mortis, Mare Ingenii and Hayn experience a systematically lower Sun elevation.

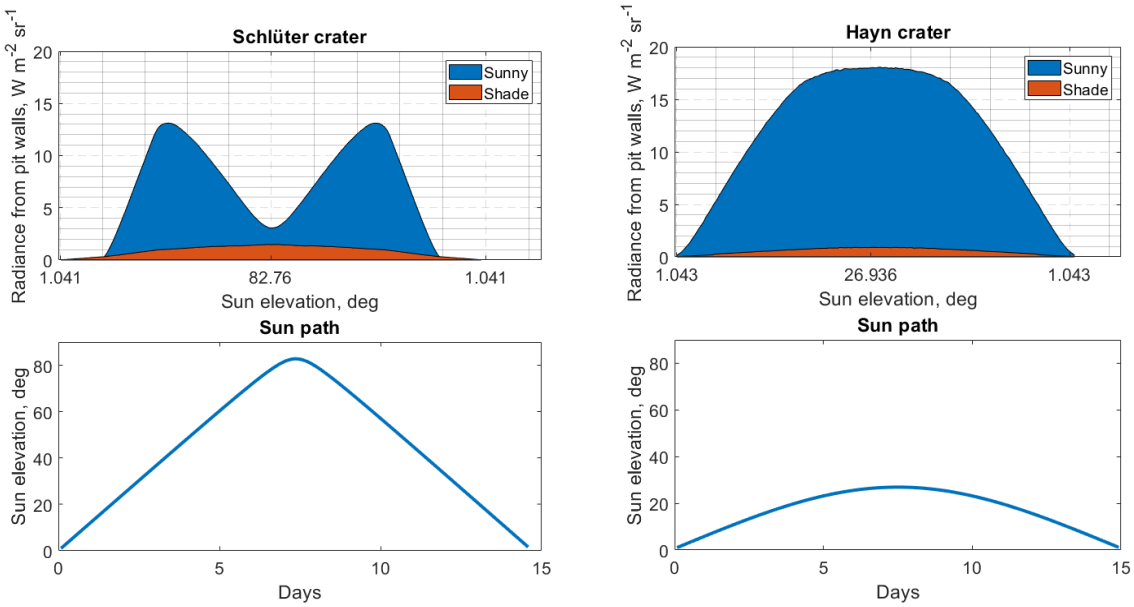

Figure 8 The difference in the radiance profile of the sunny side of the cave pits induced by the Sun elevation excursion is well visible in this comparison between the Schlüter crater (double-peak) and the Hayn crater (flat top hat).

The plausible link between the radiance values and the Sun elevation that manifests as a marked difference between the double-peak and flat top-hat profiles is graphically reproposed in Figure 9 for three Sun elevation points. When the Sun culminates almost at the Zenith (as for the C. Mare Fecunditatis, top of Figure 9) the direct illumination of the cave pit is basically zero and the light pool from the sun is projected only onto the cave base floor. This configuration is responsible for the drop in the double-peak profile of the radiance graphs in Figure 5. For smoother Sun paths over the cave like the

Hayn Crater and Lacus Mortis (centre and bottom of Figure 9) a certain portion of the cave pit is more constantly illuminated leading to the flat top-hat profile.

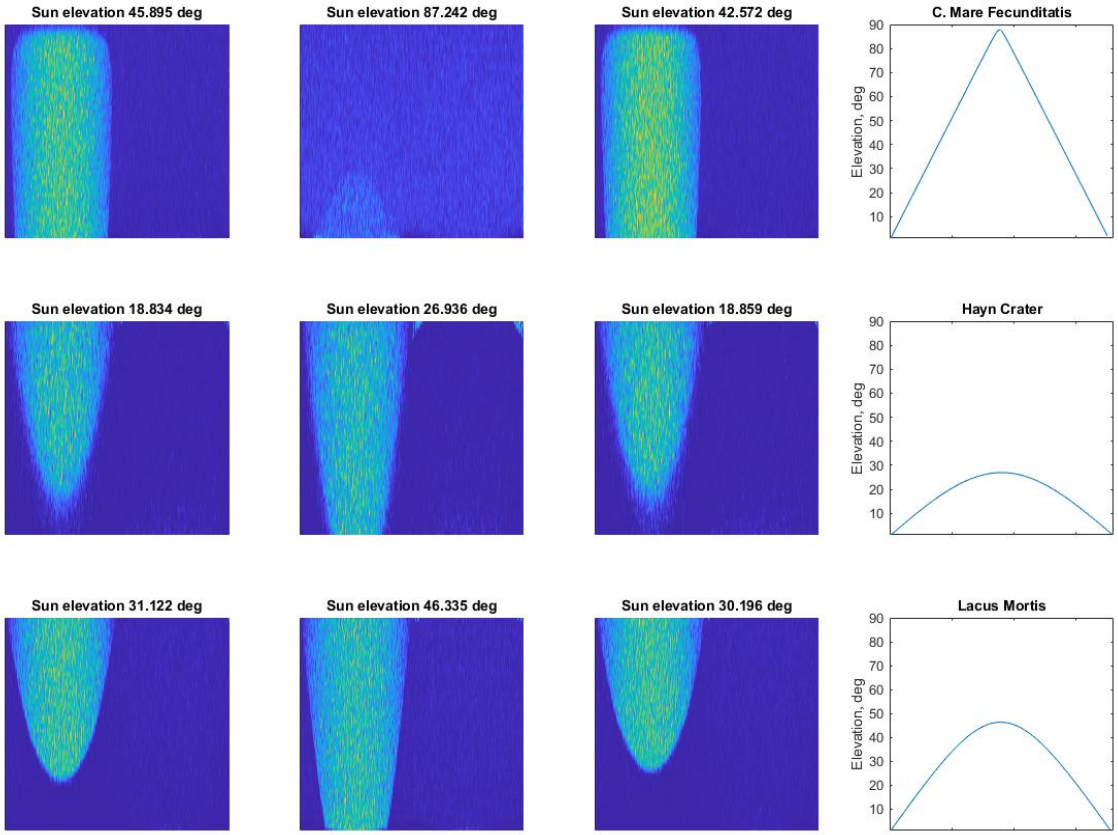

Figure 9 The Sun culmination points close to the Zenith illuminate only the base floor of the cave leading to a decrease of the scattered light from the cave pit walls as shown at top plots belonging to the C. Mare Fecunditatis. When the Sun is systematically lower as for the Hayn (centre) or Lacus Mortis (bottom) craters the fraction of the cave pit directly illuminated is more constant.

As previously stated, for the caves with an elliptical shape the orientation of the cave major and minor axes with respect to the lunar north has not been taken into account, limiting the study of the radiance properties with the Sun elevation only. However for the most elongated cave of our ensemble (Mare Ingenii Crater) we have run two simulations with opposite orientation of the cave semi-major axis with respect to the Sun, see Figure 10. The variation of the radiance of the sunny side in the two opposite configurations is in the order of ~27%. The variation of the shade side is more contained, about 15%. The amplitude and the variation of the radiance variation is therefore driven predominantly by the Sun elevation.

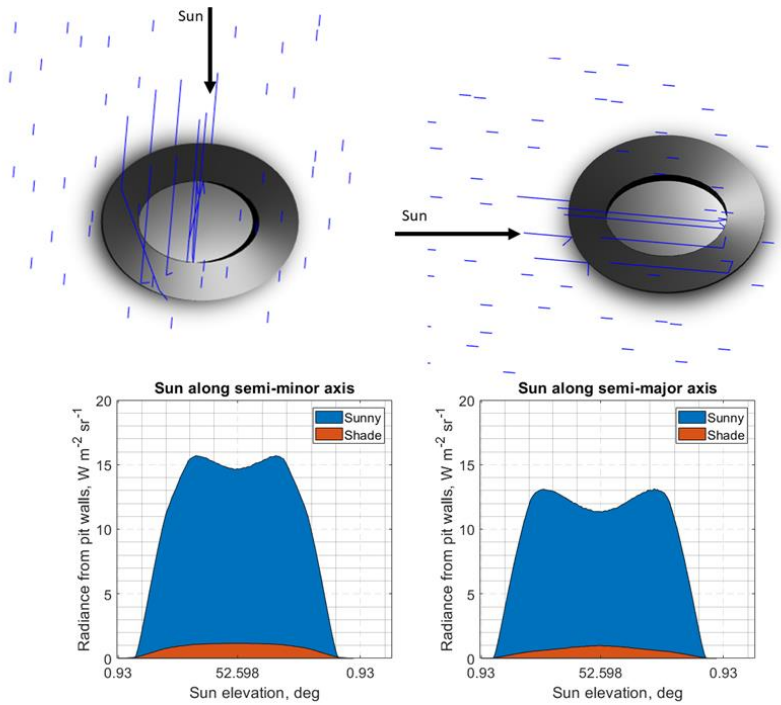

Figure 10 Comparison between the two extreme Sun-to-cave orientation cases for the Mare Ingenii cave. On the left side the Sun rays are orthogonal to the semi-major axis of the cave while on the right side the rays are parallel to the semi-major axis. The relative percentual difference in the radiance values is about 27%. The variation of the radiance on the shade side is smaller, about 15%.

The dependence of the radiance within the pit on the outer funnel geometry (inner sloping in or torus Figure 3) is studied in Figure 11. The change of the radiance from the shade side is very limited while the simulations suggest that the radiance of the sunny side is systematically higher for low and intermediary Sun elevations in the presence of a torus-like rim of the outer funnel and systematically slightly lower for high Sun elevations.

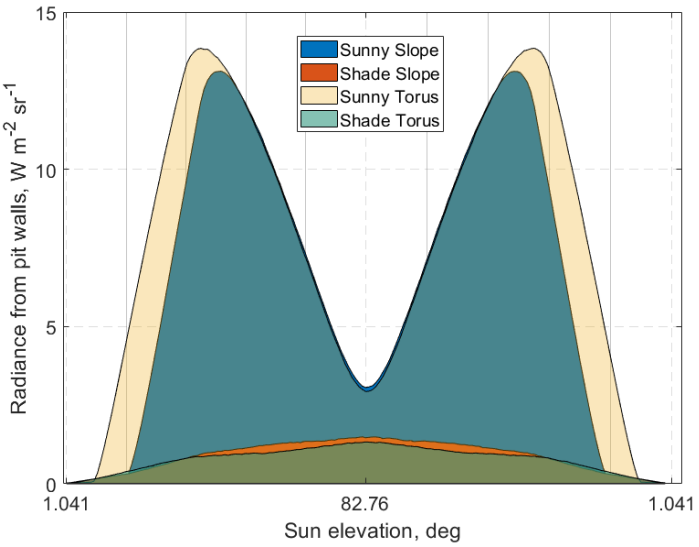

Figure 11 Simulation of the Schlüter Crater for different rim geometries: the radiance of the pit walls is higher for an outer funnel rim with a torus like shape for low and intermediary Sun elevations. The situation is reversed for high Sun elevations where the rim with a sloping in shape leads to a slightly higher radiance of both the sunny and shade sides.

An extreme case of study is represented by the Shackleton Crater located at the Moon South pole and seeing the Sun under an elevation angle of maximum 1.5 degrees. The inner part of this crater never receives direct illumination from the Sun [20] therefore it encloses a unique environment for scientific investigations. The sole radiation within the crater comes from the light scattered by the rim of the outer funnel (sloping in profile). The inner walls of the crater are modeled as a flared cylinder. The radiance map retrieved by the ray tracing simulation is given in Figure 12.

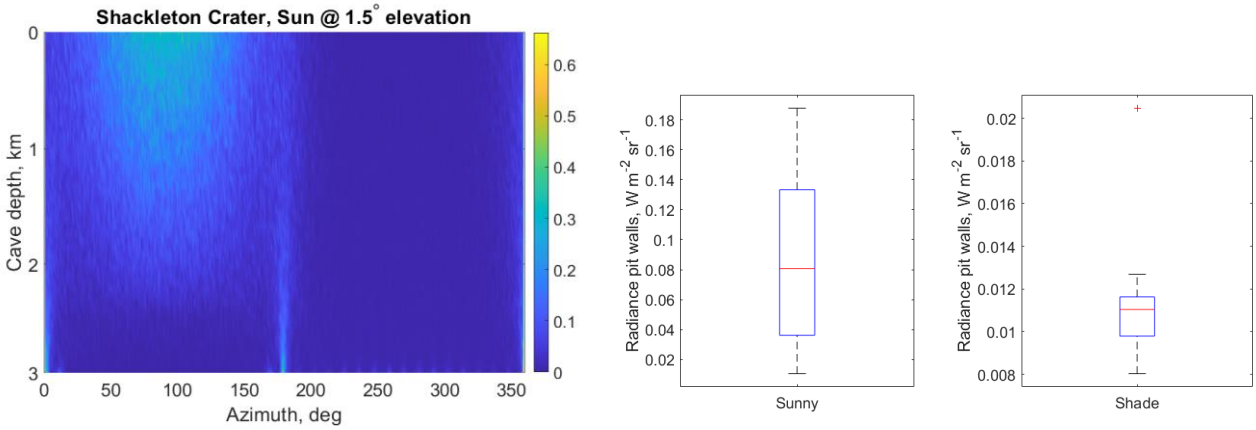

Figure 12 Left: the Shackleton Crater is located at the Moon South pole and its pit never receives direct sunlight. The only light source within the cave comes from the scattered radiation from the outer funnel. Right: statistics of the sunny and shade sides of the crater pit.

A global view of the statistics of the radiance values for the different caves is shown in Figure 13. The variation of the median of the radiance among in the different caves oscillates between 0.2-1 W m^{-2} sr^{-1} for the shade side and between 2-18 W $m^{-2}sr^{-1}$ for the sunny side of the pit.

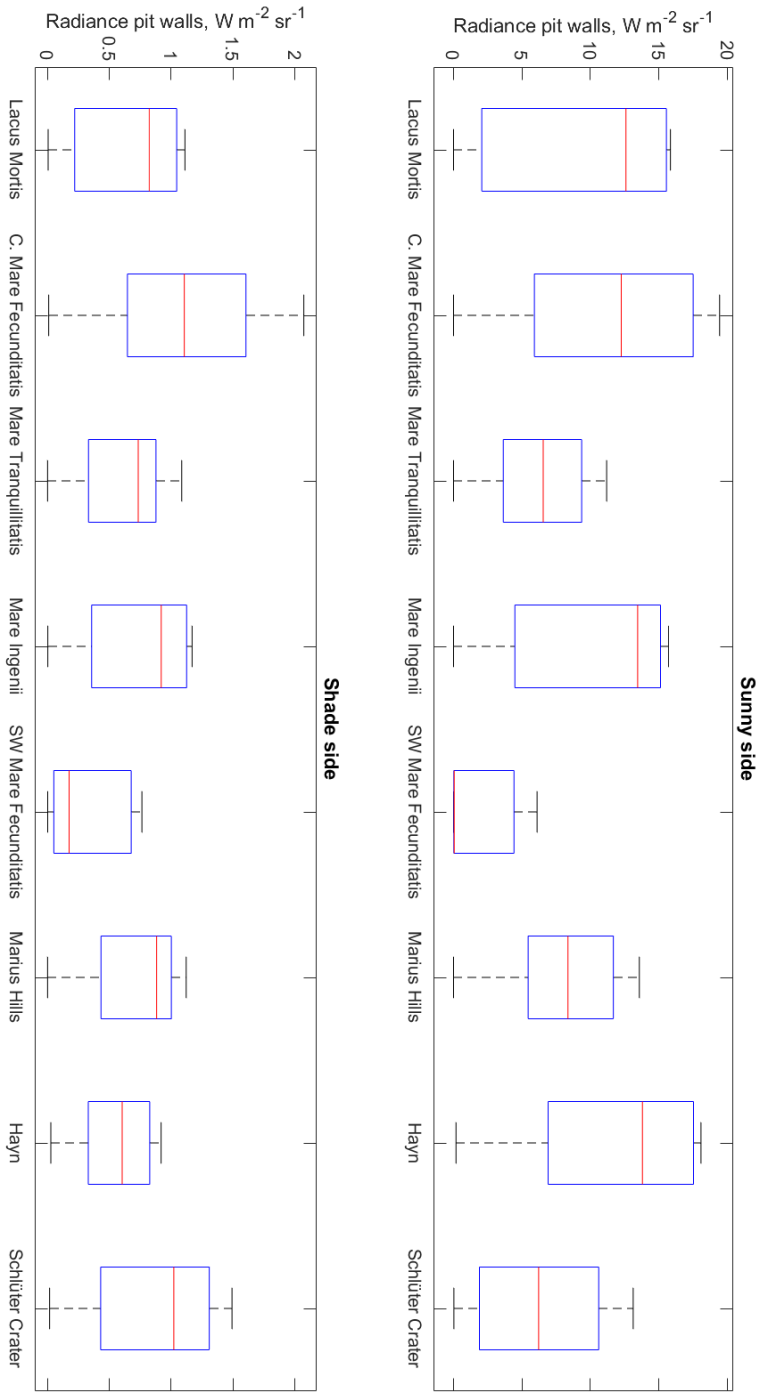

Figure 13 Collective view of the radiance statistics within the cave pit for the sunny (upper) and shade (lower) side. The data distribution is represented using a boxplot graphics showing the extremes of the range (top-bottom black bars) the 25 and 75 quantiles (blue box) and the median (red line). Assuming the median as reference value, the variation of the radiance among the different caves is relatively limited: the shade side oscillates between 0.2-1 W m^{-2} sr^{-1} and the sunny side between 2-18 W m^{-2} sr^{-1}.

5. CONCLUSIONS

With this work we have provided a simulation scheme that combining three software tools (STK, OpticStudio, Matlab ZOS-API) can setup an operational scenario to retrieve radiance maps within a lunar cave at any epoch. The ray tracing segment that is the core of the simulation work has been modelled using a non-sequential representation of the caves and a Lambertian scattering model of their inner pits. These results can be used as a ground for the SNR calculations of whatsoever instrument let down into the cave. We envision a future extension of the current work by including some scattering and reflectance profiles that mimic more faithfully the lunar regolith properties and the Sun emission spectrum. The cave geometry can be further modelled in finer details using a step/cad file of the pit orography where available.

REFERENCES

[1] A. Austin et al., Robotic Lunar Surface Operations 2, Acta Astronautica 176 (2020) 424-437, https://doi.org/10.1016/j.actaastro.2020.06.038

[2] https://www.nasa.gov/gateway/overview

[3] A. P. Rossi et al., DAEDALUS – Descent And Exploration in Deep Autonomy of Lava Underground Structures, https://doi.org/10.25972/OPUS-22791

[4] Junichi Haruyama, et al. Possible lunar lava tube skylight observed by SELENE cameras", Geophysical Research Letters, 36(21), 2009.
eprint: https://agupubs.onlinelibrary.wiley.com/doi/pdf/10.1029/2009GL040635. 11

[5] T. Kaku, et al., "Detection of Intact Lava Tubes at Marius Hills on the Moon by SELENE (Kaguya) Lunar Radar Sounder", Geophysical Research Letters, 44(20):10,155–10,161, 2017. eprint: https://agupubs.onlinelibrary.wiley.com/doi/pdf/10.1002/2017GL074998. 11

[6] Sonia Calvari and Harry Pinkerton, "Formation of lava tubes and exten- sive flow field during the 1991–1993 eruption of Mount Etna", Journal of Geophysical Research: Solid Earth, 103(B11):27291–27301, 1998. eprint: https://agupubs.onlinelibrary.wiley.com/doi/pdf/10.1029/97JB03388. 11

[7] Stephan Kempe, et al., "Inflationary versus crusted-over roofs of pyroducts (lava tunnels)", In Proceedings 14th International Symposium on Vulcanospeleology, August 2010. 11

[8] Francesco Sauro, et al, "Lava tubes on Earth, Moon and Mars: A review on their size and morphology revealed by comparative planetology", Earth-Science Reviews, 209:103288, October 2020.

[9] Audai K. Theinat, et al., "Lunar lava tubes: Morphology to structural stability", Icarus, 338:113442, March 2020.

[10] David M. Blair, et al., "The structural stability of lunar lava tubes", Icarus, 282:47–55, January 2017.

[11] Loic Chappaz, et al., "Evidence of large empty lava tubes on the Moon using GRAIL gravity", Geophysical Research Letters, 44(1):105–112, 2017. eprint: https://agupubs.onlinelibrary.wiley.com/doi/pdf/10.1002/2016GL071588.

[12] M. S. Robinson, et al., "Confirmation of sublunarean voids and thin layering in mare deposits", Planetary and Space Science, 69(1):18–27, August 2012. 13, 66

[13] D. P. Cruikshank and C. A. Wood, "Lunar rilles and hawaiian volcanic features: Possible analogues", The moon, pages 412–447, 1972. 16

[14] G. De Angelis, et al., "A radiation safety analysis for lunar lava tubes", Journal of Radiation Research, 43:2, 2002. 13, 14

[15] Junichi Haruyama, et al., "Lunar Holes and Lava Tubes as Resources for Lunar Science and Exploration", In Viorel Badescu, editor, Moon: Prospective Energy and Material Resources, pages 139–163. Springer, Berlin, Heidelberg, 2012.

[16] Spudis, P.D., et al., "Geology of Shackleton Crater and the south pole of the Moon", Geophys. Res. Lett. 35, 1–5 2008. https://doi.org/10.1029/2008GL034468

[17] Zuber, M.T., et al., "Constraints on the volatile distribution within Shackleton crater at the lunar south pole", Nature 486, 378–381. https://doi.org/10.1038/nature11216

[18] Y. Shkuratov, et al., "Optical measurements of the Moon as a tool to study its surface", Planetary and Space Science 59 (2011) 1326-1371.

[19] Robert V. Wagner, Mark S. Robinson, Distribution, formation mechanisms, and significance of lunar pits, Icarus, Volume 237, 2014, Pages 52-60, ISSN 0019-1035, https://doi.org/10.1016/j.icarus.2014.04.002.
[20] P. O'Brein and S. Byrne, Cooler than cool: doubly shadowed regions at the lunar poles, 53rd Lunar and Planetary Science Conference, 2022.
[21] K. L. Donaldson Hanna et al., Measuring and interpreting bidirectional reflectance distribution functions for Apollo lunar regolith samples using the visible Oxford space environment goniometer, 53nd Lunar and Planetary Science Conference, 2022, (LPI Contrib. No. 2548).
[22] J. L. Piatek et al., Scattering properties of planetary regolith analogs, Icarus 171 (2004) 531-545.